Intrinsic Q_p at Mt. Etna from the inversion of rise times of 2002 microearthquake sequence

Salvatore de Lorenzo [1][2]**, Marilena Filippucci** [1][2]**, Elisabetta Giampiccolo** [3] **and Domenico Patanè** [3]

[1] *Dipartimento di Geologia e Geofisica, Università degli Studi di Bari, Italy*
[2] *Centro Interdipartimentale per la Valutazione e Mitigazione del Rischio Sismico e Vulcanico, Bari, Italy*
[3] *Istituto Nazionale di Geofisica e Vulcanologia, Catania, Italy*

Abstract

About three-hundred microearthquakes, preceeding and accompanying the 2002-2003 Mt. Etna flank eruption, were considered in this study. On the high-quality velocity seismograms, measurements of the first half cycle of the wave, the so-called rise time τ, were carried out. By using the rise time method, these data were inverted to infer an estimate of the intrinsic quality factor Q_p of P waves and of the source rise time τ_0 of the events, which represents an estimate of the duration of the rupture process. Two kind of inversions were carried out. In the first inversion τ_0 was derived from the magnitude duration of the events, assuming a constant stress drop and Q_p was inferred from the inversion of reduced rise times $\tau - \tau_0$. In the second inversion both τ_0 and Q_p were inferred from the inversion of rise times. To determine the model parameters that realize the compromise between model simplicity and quality of the fit, the corrected Akaike information criterion was used. After this analysis we obtained $Q_p = 57 \pm 42$. The correlation among the inferred τ_0 and Q_p, which is caused by some events which concomitantly have high τ_0 (>30 ms) and high Q_p (>100) indicates that the technique used is able to model rise time *versus* travel time trend only for source dimensions less than about 80 m.

Key words *intrinsic quality factor – stress drop – rise time – corrected Akaike information criterion*

1. Introduction

The intrinsic quality factor Q_p of the compressional body waves is considered one of the geophysical parameters best correlated to the physical state of the rocks. This is because, as shown in laboratory studies (Kampfmann and Berckemer, 1985; Sato and Sacks, 1989) a type-

Arrhenius exponential law relates Q_p to the temperature T and the pressure P of the rocks. In volcanic areas, low Q_p values are usually associated with high temperature rocks (*e.g.*, Sanders *et al.*, 1995; de Lorenzo *et al.*, 2001). However there are several reasons which make it difficult to determine the temperature of the rocks from estimates of Q_p in the crust. First of all, Q_p depends not only on the temperature but also on the percentage of fluid content in the rocks (Bourbiè *et al.*, 1987). Morevoer, the Q_p estimates are also dependent on the technique used to retrieve them (Tonn, 1989). These considerations lead to the conclusion that only a comparison between Q_p and T in deep boreholes can help us to locally calibrate a Q_p-T relationship (*e.g.* de Lorenzo *et al.*, 2001) and then to infer the temperature field from three-dimensional images.

Some previous studies have examined the attenuation properties at Mt. Etna volcano by applying frequency domain techniques (Patanè *et al.*, 1994, 1997). The results obtained by the above studies have shown that the effect of attenuation on seismic radiation at Mt. Etna is considerable. Patanè *et al.* (1994) reported significant variations of Q from P waves as a function of depth. In particular, a drop of Q values for earthquakes located at depths less than 5 km was observed, supporting the idea that the upper part of the crust and the shallow volcanic layers are characterized by low Q. Recently a P-wave attenuation tomography study was carried out at Mt. Etna, down to 15 km of depth, using high quality data recorded in the period 1994-2001 (De Gori *et al.*, 2005). Results from this first tomography were refined in the shallow layers (around 2 km) of the volcanic edifice by Martìnez-Arevalo *et al.* (2005), further confirming significant variations of total Q as a function of depth and azimuth.

In the frame of the European project named VOLUME (an acronym of «VOLcanoes Understanding of Mass movEment») aimed to investigate the movement of fluid masses inside Mt. Etna, a research line has been dedicated to the reconstruction of Q_p images of the volcano with different techniques. This is because several studies have pointed out that the estimates of Q could depend on both the data to be inverted and on the technique used. The attenation parameter Q^{-1} estimated by the inversion of seismic spectra at Mt. Etna by De Gori *et al.* (2005) and Martìnez-Arevalo *et al.* (2005) is the sum of two parameters, Q_p^{-1} and Q_c^{-1}, which take into account two different and concomitant physical phenomena. Q_p^{-1} is the intrinsic attenuation of P waves, which is related to the losses of energy due to the anelasticity of the Earth. Q_c^{-1} is the scattering attenuation of the wave field and is related to the energy content of the secondary wave field, *i.e.* the wave field generated by the elastic heterogeneities inside the medium travelled by the waves (*e.g.*, Mitchell, 1995; Del Pezzo *et al.*, 2001). It has also been shown (*e.g.*, Liu *et al.*, 1994) that the methods based on the inversion of pulse widths of first P waves are more appropriate to estimate the intrinsic Q_p, in that only the start of the signal, which is rela-

tively free of complicated effects, such as complexities at the source and/or scattering from heterogeneities, is used.

Based on these reasonings, this article presents the results of a first study aimed to obtain a first estimate of the average intrinsic Q_p at Mt. Etna by using the classic rise time method (Gladwin and Stacey, 1974). The analysis concerns about three-hundred microearthquakes recorded at Mt. Etna preceeding and accompanying the 2002-2003 Mt. Etna flank eruption.

2. The Mt. Etna geological framework

Mt. Etna is located in the complex geodynamic framework of Eastern Sicily, where major regional structural lineaments play a key role in the dynamic processes of the volcano (*e.g.*, Patanè and Giampiccolo, 2003).

Several years of structural and geophysical observations have revealed that the orientation of most of the eruptive systems coincides with two structural trends NNW-SSE and NE-SW, observed both in the volcanic area and in the regional context (*e.g.*, Azzaro and Neri, 1992). These alignments are hypothesized as the main volcano-genetic structures (*e.g.*, Gresta *et al.*, 1998) which control the evolution of Mt. Etna, as their interference establishes a weakness volume along which magma can rise from depth (Rasà *et al.*, 1995).

Over the last 30 years Mt. Etna has had a high rate of eruptive events and therefore it constitutes one of the most important natural laboratories for the understanding of eruptive processes and lava uprising in basaltic-type volcanic environments. Seismic observations allowed us to carry out detailed investigations on major aspects of seismicity. In particular, the most recent effusive eruptions which occurred in 1989, 1991-1993, 1999, 2001 and 2002-2003 have offered good examples for quantitative analysis based on seismic data in digital format.

We focus on the 2002-2003 flank eruption which started in the night between October 26 and 27, 2002 with a seismic swarm in the central and upper part of the volcano. Fissures on both the NE and S flanks were activated with a huge lava emission and powerful explosive activity from the southern fracture field. The eruption

ended on January 28, 2003 after 94 days. More than 800 events were recorded during this period by the permanent seismic network managed by INGV. Most of these events have magnitude less than 3.0 and only few earthquakes reached a magnitude duration $M_d = 4.4$.

3. Technique

The rise time method is based on early experimental (Gladwin and Stacey, 1974) and theoretical (Kjartannson, 1979) studies. More recently, Wu and Lees (1996) showed that the theoretical relationship on which the method is based remains valid if we consider a heterogeneous anelastic structure. The most limiting assumption of this method is that it neglects the directivity effect of the seismic radiation generated by a finite dimension seismic source (Zollo and de Lorenzo, 2001).

On a velocity seismogram the rise time can be defined as the time interval between the onset of the phase and its first zero crossing time (fig. 1). If the spatio-temporal finiteness of the seismic source process can be neglected, the variation of the rise time *versus* the travel time
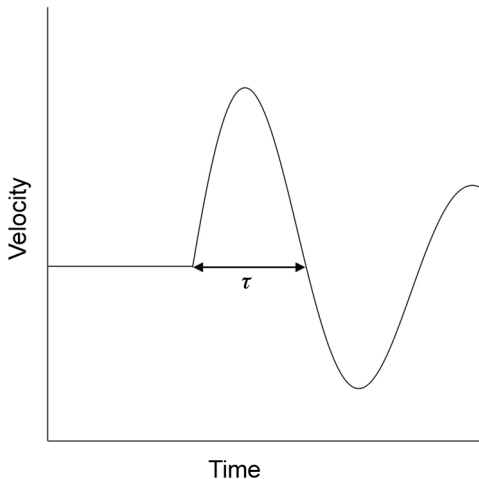
of the wave will be given by

$$\tau = \tau_0 + \frac{C}{Q_p} T \qquad (3.1)$$

where τ_0 is the rise time at the source, Q_p is the quality factor and T is the travel time. The constant C was found to be equal to 0.5 for a constant Q attenuation operator (Kjartansson, 1979).

The methods based on the inversion of the rise times are expected to give the most reliable estimates of the intrinsic attenuation (Liu *et al.*, 1994). In fact, since only a very limited portion of the seismogram is used, the effects of multiple waves generated in the thin layers around the recording site are usually minimized.

Finally, as a consequence of the point-like source assumption, the Q_p inferred by using eq. (3.1) can be considered as the minimum Q_p estimated from pulse width inversion (de Lorenzo *et al.*, 2004).

4. Data analysis

We used a data set of about 300 well located events (Erx, Ery and Erz <1 km, Gap < 100° and RMS < 0.20 s), with magnitude duration ranging between 1.4 and 4.4 and focal depth mainly concentrated in the first 5 km, recorded during an episode of intense seismic activity which preceded and accompanied the 2002-2003 Mt. Etna flank eruption. The earthquakes were selected from the catalogue among those re-located by using the most recent 3D velocity model (Cocina *et al.*, 2005). Data from stations of the Mt. Etna permanent seismic network run by Istituto Nazionale di Geofisica e Vulcanologia of Catania (INGV-CT) were analysed. Most of the stations considered in this analysis are equipped with one-component short period (1 s) sensors, except 8 equipped with three-component sensors. Although other stations were operating during the occurrence of the analysed seismic sequence, data were not as well recorded as required for accurate seismic attenuation analysis in time domain.

We discarded the events for which the rise times are available at fewer than four stations. The remaining dataset was then composed of 147 events, all having typical tectonic-earth-

Fig. 1. Schematic picture of rise time τ as measured on a velocity seismogram.
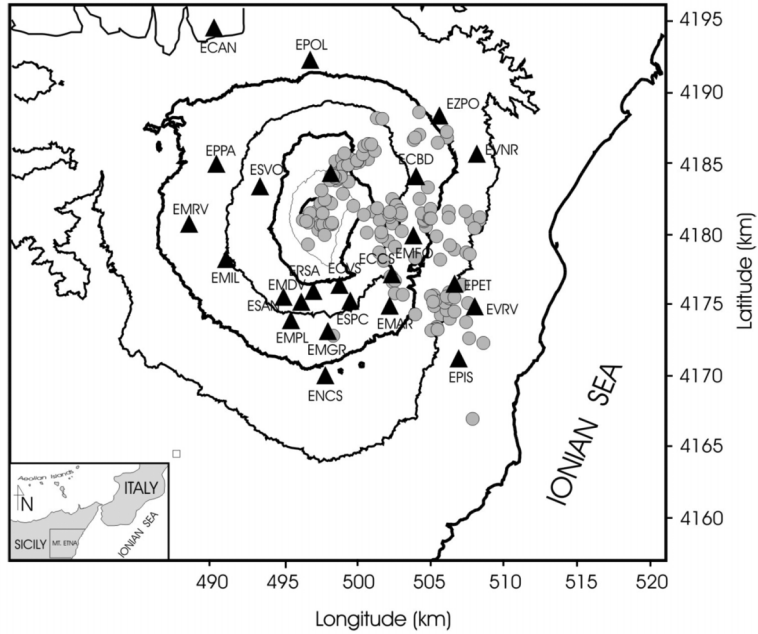
Fig. 2. Epicenters of the events (grey circles) and recording stations (black triangles) considered in this study.

Table I. The dataset available for this study. M_d = magnitude duration; Id = identification number of the event; Date = month-day-hour and minute of occurrence of the event (year: 2002).

Id#	Date	M_d	Id#	Date	M_d	Id#	Date	M_d	Id#	Date	M_d	Id#	Date	M_d
1	10262135	2.4	17	10270016	2.7	34	10270502	2.5	51	10280912	3.2	68	10291034	1.6
1	10262135	2.4	18	10270021A	2.4	35	10270521	2.6	52	10281140	3.1	69	10291035	2.9
2	10262146	2.3	19	10270021B	2.7	36	10270531	3.3	53	10281151	2.8	70	10291059	2.1
3	10262155	2.4	20	10270035	3	37	10270546	3.4	54	10281627	3	71	10291102	4
4	10262204	2.4	21	10270036	3.1	38	10270606	3.4	55	10282325	2.8	72	10291122	1.7
5	10262218	2.1	22	10270041	3.2	39	10270626	2.8	56	10290131	2.6	73	10291221	2.1
6	10262225	2.5	23	10270101	2.7	40	10270628	2.9	57	10290232	2.3	74	10291325	2.7
7	10262228	2.4	24	10270107	2.4	41	10270649	2.9	58	10290834	2.9	75	10291639	4
8	10262233	2.4	25	10270113	3.3	42	10270732	3.2	59	10290913	2.8	76	10291714	4.1
9	10262240	2.5	26	10270215	2.5	43	10271007	2.7	60	10290956	2	77	10291907	1.7
10	10262313	2.4	27	10270218	3.2	44	10271024	2.7	61	10291002	4.4	78	10292035	2
11	10262327	2.4	28	10270229	3.5	45	10271210	2.7	62	10291004	3.1	79	10292224	2.8
12	10262346	2.4	29	10270239	3.3	46	10271216	2.6	63	10291013	2.8	80	10300000	3.1
13	10262349	2.4	30	10270242	3.4	47	10271442	2.5	64	10291017	2.5	81	10300216	2
14	10270007	3.5	31	10270250	4.2	48	10271456	2.7	65	10291018	2.1	82	10300220	2.5
15	10270010	3.3	32	10270328	2.8	49	10271602	2.9	66	10291022	1.7	83	10300720	2.5
16	10270012	2.6	33	10270417	2.9	50	10271607	2.6	67	10291025	1.6	84	10301005	2.2

Table I (*continued*).

Id#	Date	M_d	Id#	Date	M_d	Id#	Date	M_d	Id#	Date	M_d	Id#	Date	M_d
85	10301006	2.5	98	10311041	3.2	111	11010929	1.7	124	11030535	2.1	137	11051646	2.6
86	10301047	2.6	99	10311122	2.4	112	11011301	1.5	125	11030536	2.5	138	11051900	2.8
87	10301321	2.8	100	10311150	1.9	113	11011532	3.1	126	11031343	2.2	139	11060628	2.1
88	10301525	3.2	101	10311224	1.5	114	11011814	1.6	127	11031344	2.4	140	11060927	1.9
89	10302113	1.9	102	10311319	1.9	115	11012219	1.6	128	11040529	1.9	141	11061640	3.2
90	10302114	2.5	103	10311325	1.9	116	11020901	3	129	11040826	1.9	142	11061642	2.7
91	10302117	1.7	104	10312002	1.9	117	11021006	2	130	11040847	2.6	143	11070616	2.7
92	10302118	1.5	105	10312108	2.3	118	11021033	1.4	131	11040956	1.9	144	11070618	2
93	10302312	1.6	106	10312209	2.3	119	11021527	1.5	132	11041048	2.4	145	11070903	2.3
94	10310640	2.4	107	11010042	2.4	120	11021539	1.7	133	11041052	3	146	11071507	2.4
95	10310651	1.9	108	11010638	2.1	121	11021709	2.8	134	11041054	3.1	147	11071635	2.6
96	10310734	1.9	109	11010857	2.7	122	11022308	2.5	135	11041117	1.3			
97	10310919	1.9	110	11010921	3	123	11030022	2.3	136	11041221	1.5			

quake waveforms, whose localizations, deduced from the INGV catalogue, are shown in fig. 2, together with the position of the recording stations. The origin time, the identification number and magnitude duration of the events used in the study, computed by INGV, are given in table I. A total of 1053 data was available for the study.

The rise time was measured on each first arrival *P*-wave by computing the time interval between the onset of the phase and its first zero crossing time. We discarded all data for which the *P* signal to noise ratio was lower than 10, and considered only the waveforms on which the onset of *P*-wave was clearly readable.

We did not perform the deconvolution for the instrumental response for the following three reasons: 1) First of all, the technique we are using does not need amplitude information. 2) Second, the effect of filtering operated in the deconvolution for the instrumental response could cause the generation of unwanted artificial signals (see Mulargia and Geller, 2003 and references therein) which could bias the rise time estimate. 3) Finally, if we exclude one datum, the observed rise times vary between 0.025 s and 0.3 s (fig. 3), to which correspond an average frequency content ranging from a minimum of about 3 Hz to a maximum of about 40 Hz. Consequently the frequency content of
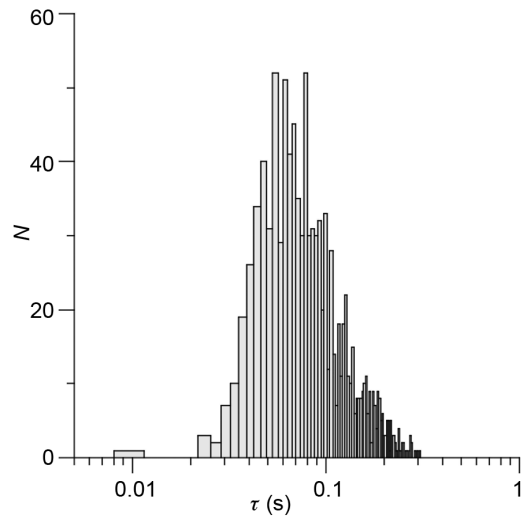
Fig. 3. Hystogram of the measured rise times.

the analyzed signals is always contained in the frequency band (1-50 Hz) where the instrument response is flat and cannot distort the duration and shape of the observed signals.

Only data not affected by multipathing during the first half-cycle of the wave were considered in the analysis. The multipathing effects
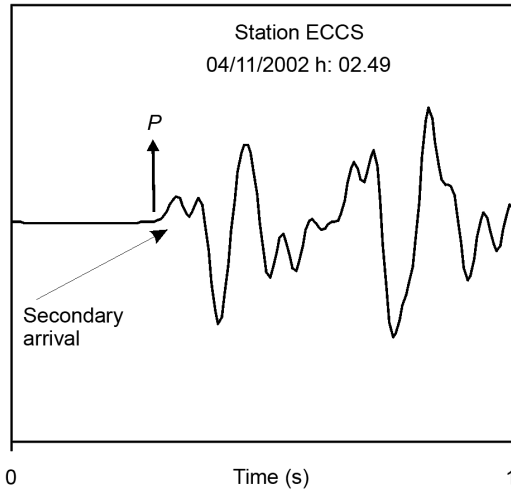
Fig. 4. A velocigram of a microearthquake occurred at Mt. Etna. The discontinuity occurring during the first half-cycle of the first *P*-wave, due to a secondary arrival, impedes the measurement of the rise time on this seismogram.

can often be easily recognized as a sharp discontinuity (*e.g.*, de Lorenzo and Zollo, 2003) which breaks the approximately bipolar shape of the wave on the velocity seismogram (fig. 4) and are generally caused by the presence of thin layers below the recording site, where part of the energy remains trapped and is subjected to multiple reflection.

The quality of the onset varies with varying the level of noise of the recorded traces. For this reason we divided the dataset into three categories. A maximum error on rise time equal to 5% was estimated for data which have the highest quality. For data of intermediate quality a maximum error of 10% was estimated. Finally, a maximum error of 20% was associated to data having the worst quality. As a consequence an average error on rise time equal to 10 ms was estimated.

The plot of the seismic rays under the assumption of a homogeneous velocity model is shown in fig. 5a,b. We infer that the central-eastern part of the array is very well illuminated by the seismic rays, until to a depth of about 3-4 km. The Q_p estimates we present in the next

section will be then particularly representative of the average Q_p of this volume.

5. Results

We carried out two different kinds of data inversions. In the first inversion we assumed that the stress drop of the studied earthquakes is a
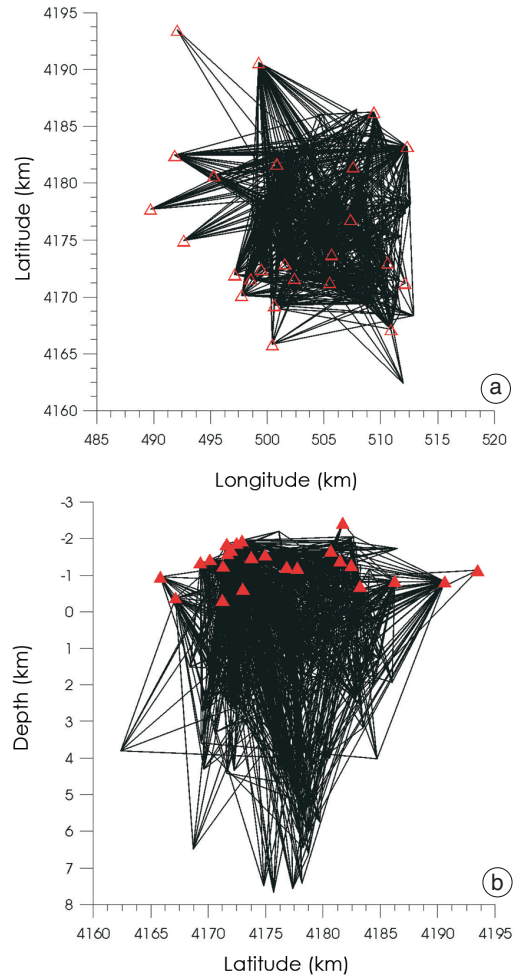
Fig. 5a,b. Plot of seismic rays available for this study: a) plot in the horizontal plane; b) plot in the vertical latitude-depth plane

constant, so that a self-similar behaviour of earthquakes with a different energy content is expected. Under this assumption the source rise time τ_0 of each event was computed by using the seismic moment *versus* magnitude duration relationship calibrated for the Etnean area (Patanè *et al.*, 1993) and the laws which relate source radius, seismic moment, stress drop, rupture velocity and source rise time for a circular crack model. In the second inversion, source rise times were directly estimated from data using the relationship (3.1).

5.1. Q_p *estimates under the assumption of a constant stress drop*

For each of the 147 considered events, seismic moment M_0 was inferred from the magnitude duration M_d (table I), using the relationship which relates M_d to M_0 for the Etnean area (Patanè *et al.*, 1993)

$$\text{Log}\, M_0 = a + b M_d \qquad (5.1)$$
$$\text{with}$$

$$a = 17.8 \pm 1.9 \qquad (5.2)$$

$$b = 0.9 \pm 0.1 . \qquad (5.3)$$

For a circular crack, the source rise time τ_0, which represents the time duration of the slipping on the fault, is related to the source radius L and the rupture velocity V_r of a circular crack by the equation (Brune, 1970)

$$\tau_0 = \frac{L}{V_r} . \qquad (5.4)$$

By combining eq. (5.4) with the relationship which combines stress drop $\Delta\sigma$, M_0 and L (Keilis-Borok, 1959)

$$\Delta\sigma = \frac{7}{16} \frac{M_0}{L^3} \qquad (5.5)$$

we obtain

$$\tau_0 = \frac{1}{V_r} \sqrt[3]{\frac{7}{16} \frac{M_0}{\Delta\sigma}} . \qquad (5.6)$$

In order to compute τ_0, we need to estimate the rupture velocity V_r of the earthquakes. Unfortunately, this parameter is poorly known for small

magnitude earthquakes, owing to its correlation with the other source parameters (*e.g.*, Deichmann, 1997). Theoretical and laboratory studies (Madariaga, 1976) indicate that V_r ranges between 0.6 V_s and 0.9 V_s. Starting from the observation of a great dispersal of rise time *versus* travel time for the considered events, which is often attributed to significant directivity effects (*e.g.*, de Lorenzo *et al.*, 2004), we have assumed a high value of the rupture velocity ($V_r = 0.9$ $V_s = 2.2$ km/s).

For the Mt. Etna $\Delta\sigma$ is known to range from a few MPa to about 100 MPa (*e.g.*, Patanè *et al.*, 1994, 1997; Patanè and Giampiccolo, 2003). For this reason, first of all we carried out five different inversions by using five possible values of $\Delta\sigma$ ($\Delta\sigma = 1, 5, 10, 50, 100$ MPa), and then we compared the results of the inversions.

To this aim, for each value of $\Delta\sigma$, source rise times τ_0 of the events were computed using eq. (5.6). Then, for each event, the reduced rise times $\tau - \tau_0$ were inferred from eq. (3.1) and inverted to estimate Q_p.

At the first step of the inversion we assumed a constant Q for the entire area. The inversion of the entire data set of rise times was performed using a weighted linear inversion scheme with weigths equal to the inverse of the variance of data. The results are summarized in fig. 6a-c. It is worth noting that about the same quality of the fit is obtained for $\Delta\sigma = 10$ MPa (an average residual of 42 ms in $L1$ norm and an average residual of 62 ms in $L2$ norm) and for $\Delta\sigma = 50$ MPa (an average residual of 42 ms in $L1$ norm and an average residual of 61 ms in $L2$ norm). The coefficient of correlation for the two cases, as computed using the relationship for weighted data (Green and Margerison, 1978) is also about the same ($R^2 = 0.24$). For this reason, Q_p was estimated by averaging the two Q_p estimates for $\Delta\sigma = 10$ MPa ($Q_p \sim 33$) and $\Delta\sigma = 50$ MPa ($Q_p \sim 30$), obtaining

$$Q_p = 32 \pm 2 . \qquad (5.7)$$

Owing to the difficulties in accurately accounting for both the errors on data and the tradeoff among source parameters, instead of fixing the stress drop to one of the values which produce the comparable fit to data ($\Delta\sigma = 10$ or $\Delta\sigma = 50$
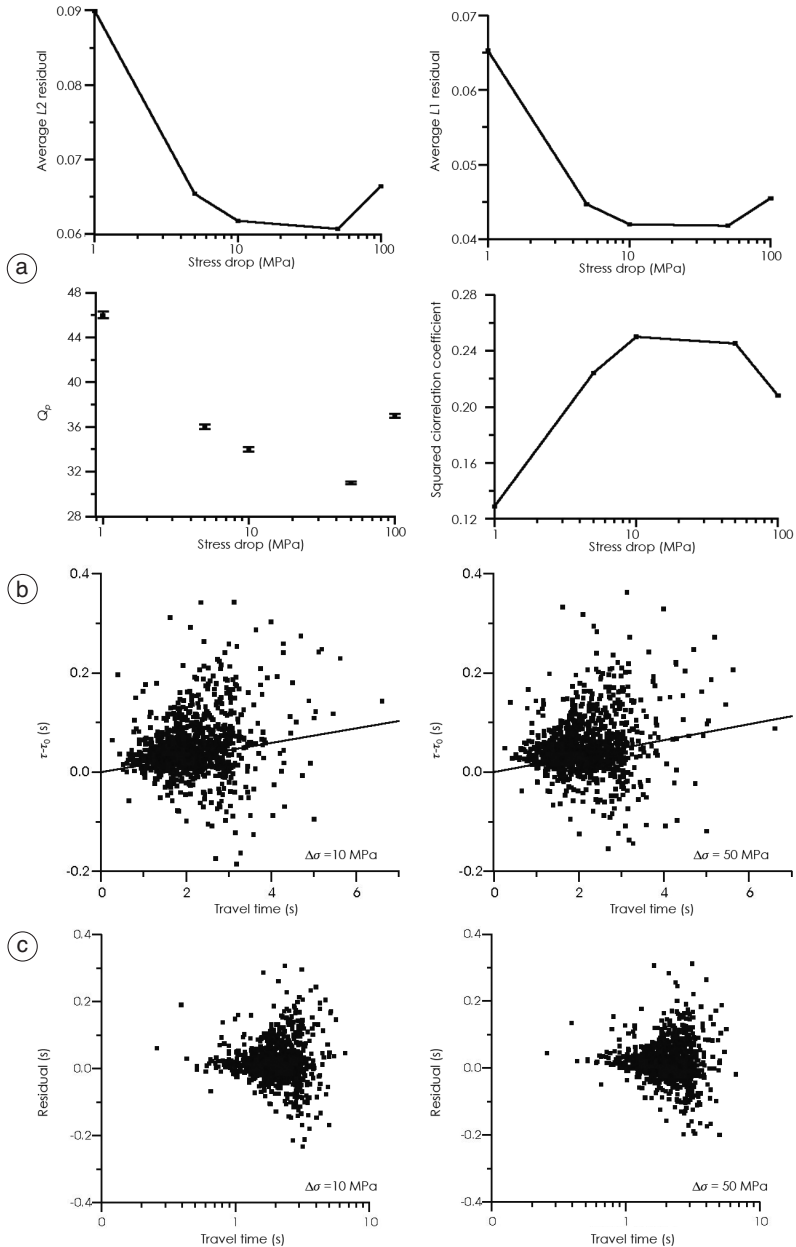
Fig. 6a-c. a) Results of the inversions of rise times for different values of $\Delta\sigma$, assuming a constant $\Delta\sigma$ and a homogeneous Q_p. On the top-left, the plot of the average residual in $L2$ norm *versus* $\Delta\sigma$ is shown. On the top-right the plot of the average residual in $L1$ norm *versus* $\Delta\sigma$ is shown. On the bottom-left the plot of average Q_p *versus* $\Delta\sigma$ is shown. On the bottom-right the plot of the squared correlation coefficient *versus* $\Delta\sigma$ is shown. b) Plot of reduced rise times *versus* travel times for $\Delta\sigma=10$ MPa and $\Delta\sigma=50$ MPa. c) Plot of rise time residuals *versus* travel times for $\Delta\sigma=10$ MPa and for $\Delta\sigma=50$ MPa under the assumption of a homogeneous Q_p.

MPa), we preferred to consider, in the calculation of Q_p of each event, both the cases $\Delta\sigma=10$ MPa and $\Delta\sigma=50$ MPa, choosing, for each event, the Q_p value which gives rise to the best fit result. Results are summarized in table II. Only two events show a negative non physical Q_p value: event #85, for which we have $Q_p=-37$ and event #100, for which we have $Q_p=-100$.

Table II. Qp estimates under the assumption of a constant stress drop.

Id	N data	Q	ΔQ	L1 residual (s)	L2 residual (s)	$\Delta\sigma$ (Mpa)	Id	N data	Q	ΔQ	L1 residual (s)	L2 residual (s)	$\Delta\sigma$ (Mpa)
1	14	21	1	43	47	50	35	7	28	2	20	23	50
2	15	24	1	15	27	10	36	9	20	2	39	47	10
3	9	30	1	12	14	50	37	13	25	2	68	89	50
4	7	26	2	18	24	10	38	9	24	1	67	91	10
5	7	24	1	26	38	10	39	6	25	1	43	69	50
6	10	25	1	27	33	10	40	7	15	1	23	32	50
7	14	31	1	28	32	10	41	5	16	1	172	200	10
8	15	37	3	53	61	50	42	4	14	1	21	39	50
9	14	31	1	23	27	10	43	4	−37	5	86	114	10
10	19	28	1	18	24	10	44	4	30	3	32	55	10
11	6	19	1	32	39	50	45	5	24	2	30	42	50
12	6	28	2	38	55	10	46	4	32	5	39	53	50
13	14	26	1	14	19	50	47	5	33	4	60	82	50
14	14	21	1	27	34	50	48	8	15	0	85	106	10
15	4	14	1	21	33	50	49	5	18	1	74	94	10
16	7	80	15	21	30	50	50	4	69	18	55	73	10
17	12	22	1	85	92	10	51	4	21	6	56	69	10
18	9	27	1	40	44	10	52	6	16	1	26	32	50
19	4	25	1	7	9	10	53	11	38	2	17	23	10
20	6	20	2	18	26	50	54	17	29	1	65	95	10
21	12	1230	100	61	74	50	55	5	25	1	16	21	50
22	6	14	1	52	66	50	56	9	28	2	48	63	10
23	4	27	3	15	19	10	57	6	32	2	10	12	50
24	5	35	4	27	39	10	58	10	−100	−20	147	170	50
25	8	35	6	156	180	10	59	11	23	1	31	41	10
26	4	37	3	63	86	10	60	6	21	1	18	41	10
27	10	19	1	36	45	50	61	12	29	1	58	70	50
28	5	19	1	30	52	50	62	14	23	1	77	88	50
29	6	23	2	76	96	50	63	5	34	2	25	40	10
30	6	26	3	41	74	50	64	4	35	2	9	12	50
31	9	96	2	124	173	50	65	11	31	1	17	24	50
32	7	28	3	21	33	50	66	5	35	2	14	18	50
33	7	12	1	28	41	10	67	5	41	2	9	13	10
34	7	18	1	65	88	10	68	4	18	1	17	22	10

Table II (*continued*).

Id	N data	Q	ΔQ	$L1$ residual (s)	$L2$ residual (s)	$\Delta\sigma$ (Mpa)	Id	N data	Q	ΔQ	$L1$ residual (s)	$L2$ residual (s)	$\Delta\sigma$ (Mpa)
69	11	27	1	11	17	10	109	7	39	2	7.4	9.3	50
70	10	25	1	19	24	10	110	11	31	1	15.2	20.1	50
71	7	16	1	46	62	50	111	4	47	5	34.9	48.6	10
72	8	33	1	7	9	50	112	4	44	4	21.2	28.8	10
73	4	29	1	3	3	50	113	5	22	1	28.3	35.9	10
74	5	23	2	53	77	10	114	5	45	3	5.8	9	10
75	8	32	3	100	111	50	115	4	25	2	19.0	25.6	50
76	4	25	1	50	99	50	116	4	20	2	39.1	47.3	50
77	6	43	2	5	7	10	117	8	44	2	11	15.3	10
78	7	31	1	37	45	50	118	5	45	2	4.3	6.1	50
79	10	35	1	13	17	50	119	5	26	2	32.900	38.2	10
80	9	12	1	17	26	50	120	4	31	3	41.900	50.6	10
81	7	36	2	21	27	50	121	12	31	1	17.700	23.6	10
82	5	33	4	76	97	10	122	15	35	1	9.700	12.3	50
83	9	18	1	7	9	10	123	5	31	2	12.600	20.1	50
84	5	47	2	32	66	50	124	5	21	1	15.500	23.3	10
85	7	53	4	24.0	30.8	50	125	8	19	1	34.600	49.4	50
86	5	64	12	37.3	44.4	10	126	4	18	2	12.300	20	10
87	4	27	2	10.7	16.8	10	127	4	36	6	57	101	50
88	9	26	2	48.0	58.5	10	128	4	48	4	12	15	50
89	6	38	3	9.6	15	50	129	5	23	1	25	31	10
90	13	26	1	59.2	65.8	10	130	8	34	1	10	13	10
91	4	25	1	6.8	13.5	50	131	4	26	5	4	6	10
92	5	31	2	9.0	14.4	50	132	4	30	2	3	4	10
93	6	36	4	8.3	10.6	10	133	12	22	1	15	23	10
94	6	32	1	14.8	19.3	10	134	12	22	1	31	47	10
95	6	24	1	7.2	12.1	10	135	5	33	2	17	24	10
96	5	32	2	9.2	13.2	50	136	6	21	1	45	59	50
97	6	53	4	13.6	19.1	50	137	4	26	5	21	25	10
98	13	24	1	51.6	81	10	138	5	19	2	55	90	10
99	10	32	1	27.1	37	50	139	4	17	1	12	17	50
100	4	30	2	3.0	5.1	10	140	4	46	5	11	15	10
101	6	28	1	6.2	8.5	50	141	4	9	1	50	63	10
102	5	35	3	7.7	11	50	142	5	10	1	36	47	10
103	5	15	1	37.6	56.1	10	143	13	32	1	25	32	10
104	5	23	1	9.7	18.7	50	144	7	29	2	13	15	10
105	4	27	2	21.7	29.9	10	145	5	18	1	11	13	10
106	7	30	1	7.5	10.3	10	146	7	33	2	23	30	10
107	5	19	1	9.6	12.5	50	147	4	16	1	11	14	50
108	5	32	2	12.1	15.2	10							

Moreover, only event #21 shows a very high value (Q_p=1230). For the remaining events the Q_p variations are more limited, with a minimum Q_p=9 and a maximum Q_p=96. The weighted average of Q_p, using the results of all the 147 inversions and as weights the inverse of the residuals in $L1$ norm is exactly the same as the Q_p obtained at the first inversion step

$$Q_p = 32 \pm 2 . \qquad (5.8)$$

However, with respect to the previous result, based on the assumption of a homogeneous Q_p, the assumption of a heterogenous Q structure gives rise to a further variance reduction. In fact the average residual is now 34 ms in $L1$ norm (a residual reduction of 19%) and 53 ms in $L2$ norm (a residual reduction of about 13%). The

trend of residuals *versus* travel time is shown in fig. 7a.

5.2. *Joint estimation of τ_0 and Q_p*

In another attempt we inverted the rise times to jointly infer τ_0 and Q_p of each event.

In a first inversion run, we used a linear weighted inversion scheme, with weights equal to the inverse of the variance of data. Unfortunately this approach does not allow us to impose positivity constraints on τ_0 and Q_p. For this reason, after the inversions, only for some events we inferred positive values of both τ_0 and Q_p, reported in table III. To overcome the problem of negative values of τ_0 and/or Q_p for the remaining events, we used a non linear in-
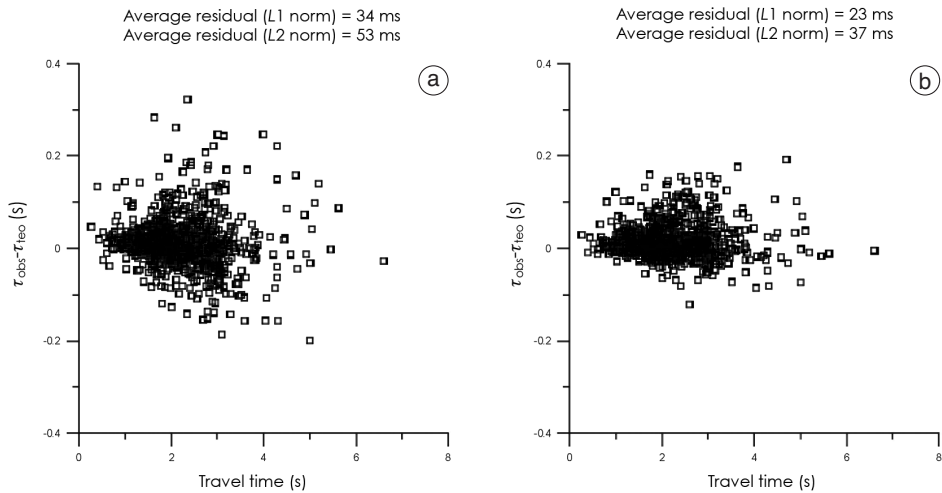
Fig. 7a,b. a) Plot of rise time residuals *versus* travel times under the assumption of a constant $\Delta\sigma$ and a heterogeneous Q_p. b) Plot of rise time residuals *versus* travel times after the joint inversion of τ_0 and Q_p.

Table III. τ_0 and Q_p estimates of the events; the lines with bold characters indicates the events for which the Simplex method has been used to overcome the problem of negative τ_0 and Q_p values.

Id	N data	τ_0 (s)	$\Delta\tau_0$ (s)	Q	ΔQ	$L1$ residual (s)	$L2$ residual (s)	Id	N data	τ_0 (s)	$\Delta\tau_0$ (s)	Q	ΔQ	$L1$ residual (s)	$L2$ residual (s)
1	14	33	3	22	1	20	28	3	9	43	3	74	19	12	15
2	15	51	2	53	9	13	17	**4**	**7**	**33**	**1**	**23**	**2**	**17**	**19**

Table III (*continued*).

Id	N data	τ_0 (s)	$\Delta\tau_0$ (s)	Q	ΔQ	L1 residual (s)	L2 residual (s)	Id	N data	τ_0 (s)	$\Delta\tau_0$ (s)	Q	ΔQ	L1 residual (s)	L2 residual (s)
5	7	69	2	393	36	13	17	**45**	**5**	**41**	**19**	**30**	**0**	**58**	**70**
6	10	76	4	571	77	18	20	**46**	**4**	**38**	**14**	**41**	**4**	**33**	**44**
7	**14**	**33**	**1**	**25**	**57**	**14**	**21**	**47**	**5**	**36**	**9**	**17**	**1**	**49**	**64**
8	15	83	3	194	99	17	26	48	8	44	7	31	3	35	44
9	14	71	3	147	42	14	21	**49**	**5**	**47**	**4**	**17**	**1**	**50**	**66**
10	19	59	3	77	17	20	25	**50**	**4**	**38**	**6**	**25**	**24**	**29**	**50**
11	6	12	5	14	1	25	33	51	4	26	2	6	0	10	18
12	**6**	**33**	**4**	**25**	**2**	**19**	**32**	52	6	78	1	112	18	18	38
13	**14**	**33**	**2**	**31**	**10**	**16**	**22**	53	11	30	4	30	3	21	30
14	14	83	4	35	4	24	31	**54**	**17**	**51**	**8**	**20**	**2**	**49**	**68**
15	**4**	**62**	**1**	**17**	**0**	**34**	**53**	55	5	43	1	55	6	8	10
16	**7**	**38**	**1**	**100**	**2**	**12**	**16**	56	9	53	3	32	3	20	28
17	12	19	9	15	3	42	55	**57**	**6**	**31**	**2**	**100**	**1**	**17**	**22**
18	**9**	**33**	**3**	**25**	**5**	**22**	**28**	**58**	**10**	**47**	**2**	**50**	**10**	**41**	**57**
19	4	15	1	16	0	6	8	**59**	**11**	**44**	**2**	**25**	**5**	**23**	**27**
20	6	59	1	59	5	13	19	60	6	17	2	17	1	25	52
21	12	65	2	349	136	12	17	**61**	**12**	**133**	**3**	**100**	**21**	**41**	**53**
22	6	90	3	42	3	17	25	62	14	63	2	20	1	27	35
23	4	32	4	25	1	12	23	63	5	15	2	20	1	15	22
24	**5**	**33**	**6**	**25**	**1**	**30**	**41**	**64**	**4**	**36**	**2**	**100**	**2**	**12**	**17**
25	**8**	**62**	**9**	**20**	**0**	**68**	**84**	65	11	9	4	18	1	25	39
26	**4**	**36**	**17**	**29**	**1**	**43**	**81**	**66**	**5**	**21**	**6**	**32**	**2**	**17**	**23**
27	**10**	**58**	**7**	**17**	**2**	**30**	**45**	67	5	4	4	24	2	7	14
28	**5**	**62**	**10**	**22**	**2**	**29**	**54**	68	4	51	3	45	5	13	23
29	**6**	**62**	**14**	**21**	**2**	**53**	**65**	69	11	88	2	241	30	11	14
30	**6**	**67**	**36**	**25**	**3**	**48**	**89**	70	10	44	2	37	3	13	23
31	**9**	**116**	**27**	**100**	**0**	**44**	**64**	71	7	10	7	12	0	31	48
32	**7**	**44**	**10**	**30**	**5**	**34**	**49**	72	8	27	1	56	5	7	8
33	**7**	**47**	**13**	**17**	**4**	**74**	**93**	73	4	14	1	22	1	5	6
34	**7**	**36**	**13**	**17**	**29**	**54**	**71**	**74**	**5**	**41**	**3**	**23**	**5**	**36**	**56**
35	**7**	**38**	**6**	**29**	**1**	**32**	**41**	**75**	**8**	**101**	**11**	**18**	**1**	**71**	**79**
36	**9**	**62**	**6**	**14**	**4**	**29**	**35**	76	4	51	13	26	2	53	103
37	**13**	**67**	**22**	**22**	**4**	**60**	**78**	**77**	**6**	**21**	**1**	**54**	**22**	**8**	**10**
38	**9**	**67**	**6**	**18**	**0**	**47**	**59**	78	7	25	3	31	3	14	20
39	6	22	15	18	2	35	60	79	10	20	2	28	1	11	13
40	**7**	**47**	**10**	**17**	**0**	**68**	**81**	80	9	160	6	42	9	19	26
41	**5**	**47**	**27**	**17**	**1**	**84**	**100**	81	7	32	4	45	9	21	31
42	**4**	**58**	**19**	**17**	**1**	**70**	**98**	82	5	56	2	20	1	14	21
43	**4**	**41**	**10**	**50**	**0**	**55**	**96**	83	9	60	2	29	3	12	17
44	**4**	**41**	**16**	**29**	**0**	**56**	**87**	**84**	**5**	**29**	**25**	**100**	**3**	**42**	**80**

Table III (*continued*).

Id	N data	τ_0 (s)	$\Delta\tau_0$ (s)	Q	ΔQ	L1 residual (s)	L2 residual (s)	Id	N data	τ_0 (s)	$\Delta\tau_0$ (s)	Q	ΔQ	L1 residual (s)	L2 residual (s)
85	7	24	2	34	3	14	17	**117**	**8**	**25**	**1**	**50**	**1**	**10**	**18**
86	**5**	**38**	**1**	**50**	**0**	**21**	**29**	118	5	39	2	130	30	5	7
87	**4**	**24**	**3**	**29**	**2**	**11**	**13**	**119**	**5**	**18**	**2**	**18**	**1**	**11**	**17**
88	9	64	1	46	4	31	44	**120**	**4**	**21**	**4**	**17**	**2**	**12**	**20**
89	**6**	**24**	**2**	**30**	**85**	**13**	**18**	121	12	49	1	70	9	19	28
90	13	17	3	18	1	24	36	122	15	24	2	26	1	9	14
91	**4**	**21**	**5**	**30**	**1**	**17**	**24**	**123**	**5**	**31**	**2**	**41**	**0**	**20**	**31**
92	5	0	2	19	1	10	14	124	5	60	1	52	3	7	9
93	**6**	**19**	**1**	**34**	**0**	**18**	**22**	125	8	55	2	43	5	18	32
94	**6**	**33**	**5**	**35**	**0**	**21**	**27**	126	4	53	0	26	1	10	13
95	6	46	0	162	22	3	4	**127**	**4**	**33**	**2**	**100**	**0**	**46**	**91**
96	**5**	**24**	**2**	**37**	**0**	**13**	**18**	**128**	**4**	**24**	**1**	**36**	**3**	**11**	**13**
97	**6**	**24**	**2**	**100**	**0**	**19**	**25**	**129**	**5**	**24**	**1**	**22**	**6**	**9**	**14**
98	13	58	2	25	1	21	30	**130**	**8**	**38**	**1**	**50**	**0**	**18**	**22**
99	10	20	4	19	1	22	35	131	4	33	1	29	1	6	9
100	4	36	1	119	9	4	6	132	4	23	1	32	1	5	7
101	6	38	1	101	23	6	8	133	12	93	2	102	15	10	14
102	5	24	2	38	3	6	9	134	12	106	4	129	49	20	26
103	5	51	1	137	39	12	17	135	5	39	3	263	112	18	35
104	**5**	**24**	**1**	**20**	**1**	**18**	**21**	136	6	55	3	335	45	22	40
105	4	31	5	25	6	22	27	137	4	28	1	17	0	13	18
106	7	47	2	37	3	9	12	**138**	**5**	**44**	**6**	**17**	**31**	**48**	**79**
107	5	7	1	14	0	11	22	139	4	38	1	35	1	12	19
108	**5**	**27**	**4**	**35**	**0**	**17**	**24**	140	4	29	1	57	4	13	18
109	**7**	**41**	**1**	**100**	**21**	**7**	**8**	141	4	27	2	7	0	34	61
110	11	47	2	75	12	16	19	142	5	114	1	50	4	29	45
111	**4**	**21**	**3**	**40**	**10**	**17**	**28**	143	13	53	4	79	17	24	31
112	4	41	2	141	18	11	18	**144**	**7**	**25**	**1**	**30**	**1**	**19**	**25**
113	5	24	6	25	2	25	40	145	5	73	2	104	21	9	12
114	5	19	1	50	1	7	12	**146**	**7**	**33**	**3**	**42**	**9**	**22**	**33**
115	**4**	**19**	**1**	**35**	**1**	**14**	**19**	147	4	72	4	116	32	16	22
116	4	116	3	213	41	18	34								

version scheme based on the use of the Simplex Downhill method (Press *et al.*, 1989) which allowed us to impose positivity constraints on both τ_0 and Q_p. To estimate the error on the inferred model parameters we applied a statistical approach based on the use of the random deviates (Vasco and Johnson, 1998). This consists of computing N_{rand} datasets by adding to each data a random quantity selected in the range of the error affecting them. The inversion results of the N_{rand} datasets can then be used to estimate the average values of the model parameters and

their standard deviations. The inversion results are summarized in table III. After this analysis we inferred Q_p values ranging from a minimum of 6 to a maximum of 570. The weighted average Q_p, with weights equal to the inverse of the average residual in $L1$ norm, was

$$Q_p = 68 \pm 51. \qquad (5.9)$$

A further variance reduction was obtained with respect to the previous case of a heterogeneous Q_p but a constant stress drop $\Delta\sigma$. In fact the average residual in $L1$ norm is now equal to 23 ms (a residual reduction of 33%) and the average residual in $L2$ norm is equal to 37 (a residual reduction of 30%). The trend of residuals *versus* travel times is shown in fig. 7b.

5.3. *Application of the «Occam razor principle»*

One point that needs to be addressed concerns the evaluation of the statistical significance of the two models used to fit data. Since the two models are characterized by a different number of model

parameters it is important establish, for each event, what of them satisfy the so called Occam's razor principle, *i.e.* realizes the best compromise between the quality of the fit and the simplicity of the model. To solve this problem we used the corrected Akaike Information Criterion (AICc) (Cavanaugh, 1997; Cavanaugh and Shimway, 1998), which represents a modified version of the Akaike (1974) criterion, to account for incompleteness of data. This consists of comparing, for the two models, the value of the parameter

$$AICc = -2\log L + 2k - \frac{k(k+1)}{(n-k-1)} \qquad (5.10)$$

where k is the number of model parameters, n the number of data and L represents the likelihood function, given by

$$L = \prod_{i=1}^{n} \frac{1}{\sqrt{2\pi}\sigma_i} \exp\left[-\frac{(\tau_{obs} - \tau_{teo})^2}{2\sigma_i^2}\right]. \qquad (5.11)$$

The model which gives rise to the minimum AICc has then to be considered the most significant from a statistical point of view.

Table IV. Application of the corrected Akaike information criterion to the two considered models. AICc1 = value of the Akaike information criterion for the model with one model parameter (only Q_p); AICc2 = value of the Akaike information criterion for the model with two model parameters (τ_0 and Q_p); ΔAICc = AICc1-AICc2.

Id# event	AICc1	AICc2	ΔAICc	Id# event	AICc1	AICc2	ΔAICc	Id# event	AICc1	AICc2	ΔAICc	Id# event	AICc1	AICc2	ΔAICc
1	391	18	373	15	−20	−12	−8	29	212	69	144	43	194	42	153
2	−9	−13	4	16	35	−19	53	30	−23	−18	−6	44	−19	7	−26
3	12	56	−45	17	2379	137	2242	31	2653	5832	−3178	45	0	7	−7
4	1	−6	7	18	505	177	328	32	−31	0	−31	46	18	148	−129
5	214	3	211	19	−28	−36	9	33	−23	30	−53	47	20	98	−78
6	196	−6	202	20	−29	−36	7	34	160	87	73	48	318	179	139
7	339	1	338	21	777	−63	841	35	−20	40	−60	49	123	34	89
8	816	26	789	22	7	−31	38	36	4	−28	32	50	115	81	34
9	161	−5	167	23	−23	−31	8	37	213	229	−17	51	3	586	−583
10	132	92	40	24	9	6	4	38	342	66	275	52	72	461	−389
11	119	−16	135	25	643	49	594	39	39	9	30	53	80	354	−274
12	59	40	19	26	222	22	200	40	−11	121	−132	54	924	942	−18
13	−30	−24	−6	27	56	66	−10	41	1362	195	1167	55	123	34	89
14	34	46	−12	28	−9	−10	1	42	−23	21	−43	56	518	935	−417

Table IV (*continued*).

| Id# event	AICc1	AICc2	ΔAICc	Id# event	AICc1	AICc2	ΔAICc	Id# event	AICc1	AICc2	ΔAICc	Id# event	AICc1	AICc2	ΔAICc
57	47	512	−465	80	−40	−41	1	103	200	−10	210	126	−25	−27	2
58	3974	126	3848	81	34	41	−6	104	−29	4	−32	127	4	−16	19
59	189	173	16	82	125	−27	152	105	−3	3	−5	128	28	−4	32
60	−41	651	−692	83	−53	−51	−2	106	−47	−44	−2	129	125	−22	147
61	1053	494	559	84	−7	71	−78	107	−33	−33	0	130	15	123	−109
62	1096	252	845	85	299	58	241	108	22	71	−49	131	−27	−31	5
63	7	212	−205	86	25	−4	29	109	11	−15	27	132	−30	−34	3
64	18	98	−80	87	−20	−22	2	110	112	121	−9	133	−45	−67	22
65	14	117	−102	88	424	94	330	111	31	−11	43	134	65	−23	88
66	16	−1	17	89	−4	30	−34	112	66	−33	98	135	28	3	25
67	−23	561	−584	90	1718	44	1674	113	1	−25	27	136	303	−17	320
68	74	75	−1	91	−33	−4	−29	114	−37	−32	−5	137	−17	−29	13
69	23	449	−426	92	−33	−13	−20	115	57	61	−4	138	23	9	14
70	173	93	80	93	−31	−18	−13	116	62	−30	92	139	13	−26	38
71	−5	1055	−1060	94	54	129	−75	117	114	112	2	140	−25	−32	7
72	45	46	−2	95	−38	−55	17	118	−27	−24	−3	141	0	−25	26
73	−33	203	−236	96	−10	76	−85	119	96	−22	118	142	29	−26	55
74	25	−7	32	97	10	100	−90	120	233	6	227	143	130	187	−56
75	514	246	269	98	204	−2	206	121	237	81	157	144	−37	−11	−27
76	−2	−8	6	99	222	90	132	122	−40	−19	−21	145	1	−30	30
77	−18	17	−35	100	−33	−39	6	123	44	167	−123	146	68	57	11
78	771	126	645	101	−5	4	−9	124	−23	−28	5	147	−12	10	−22
79	143	22	121	102	−31	−38	7	125	46	−31	77				

Table IV summarizes the comparison between the AICc values for the two considered models. In this way we were able to infer that, for 59 events the above choice of retrieving source rise times assuming a constant stress drop produces a better fit of data, whereas for the remaining 68 events the source rise times are better constrained from the inversion of rise times. By averaging the Q_p estimates obtained with this analysis we finally obtained

$$Q_p = 57 \pm 42 . \qquad (5.12)$$

Figure 8 shows the trend of the Q_p of each event estimated with the AICc as a function of τ_0. It is worth noting that a residual correlation among τ_0 and Q_p is inferred.

6. Discussion and conclusions

As thoroughly debated in Wu and Lees (1996) and de Lorenzo (1998), the slope C of the straight line interpolating τ *versus* Q_p^{-1} depends on the frequency content of the source; by calibrating eq. (3.1) with different source time functions, Wu and Lees (1996) showed that $C = 0.5$ has to be adopted if it is assumed that the the signal generated at the source has a Gaussian shape, which is a smooth representation of the unipolar source time function generated by a circular crack. By taking into account that a more realistic source cannot have the same low-frequency content as the Gaussian function, Wu and Lees (1996) showed that the C could be slightly higher. They estimated as
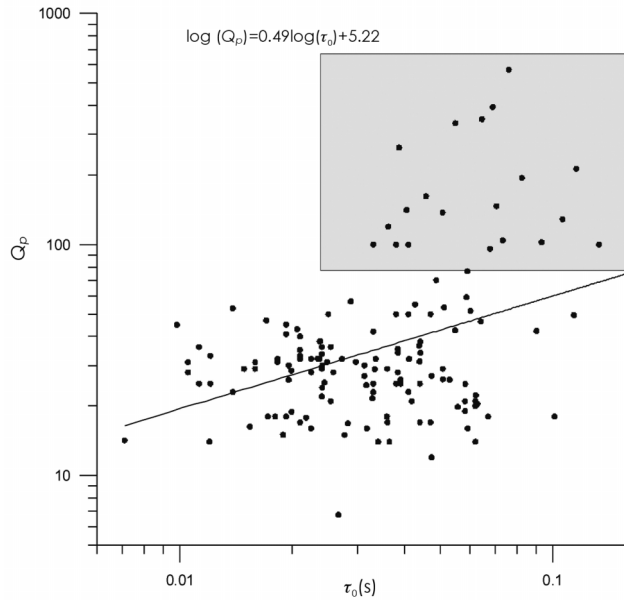
Fig. 8. Plot of Q_p *versus* τ_0 of the studied events after the application of the AICc. The points enclosed in the grey rectangle are mainly responsible for the observed correlation.
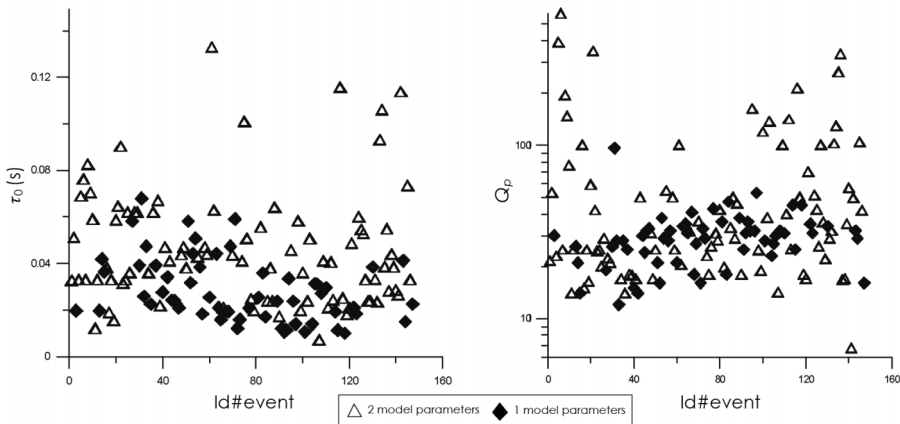
Fig. 9. Plot of τ_0 *versus* the identification number of the event and of Q_p *versus* the identification number of the event.

upper limit the value $C=0.65$. If we assume $C=0.65$, instead of $Q_p=57\pm42$ we obtain a slightly higher Q_p value ($Q_p=74\pm55$).

Let us consider now the residual correlation between Q_p and τ_0. First, we note that the Q_p es-

timate obtained using the AICc ($Q_p=57\pm42$) is intermediate between the Q_p estimate obtained under the assumption of a constant stress drop and that obtained by jointly retrieving τ_0 and Q_p. However, this result does not necessarily im-

ply a departure from the constancy of the energy release per seismic moment, nor is it necessarily caused by a great heterogeneity in the attenuating properties of the area, as one can suppose by taking into account the high value of the

standard deviation on Q_p. A possible interpretation of the correlation between Q_p and τ_0 may be that, in many cases, the data available are not sufficient to correctly estimate the two parameters. As an example, it can be easily demonstrat-
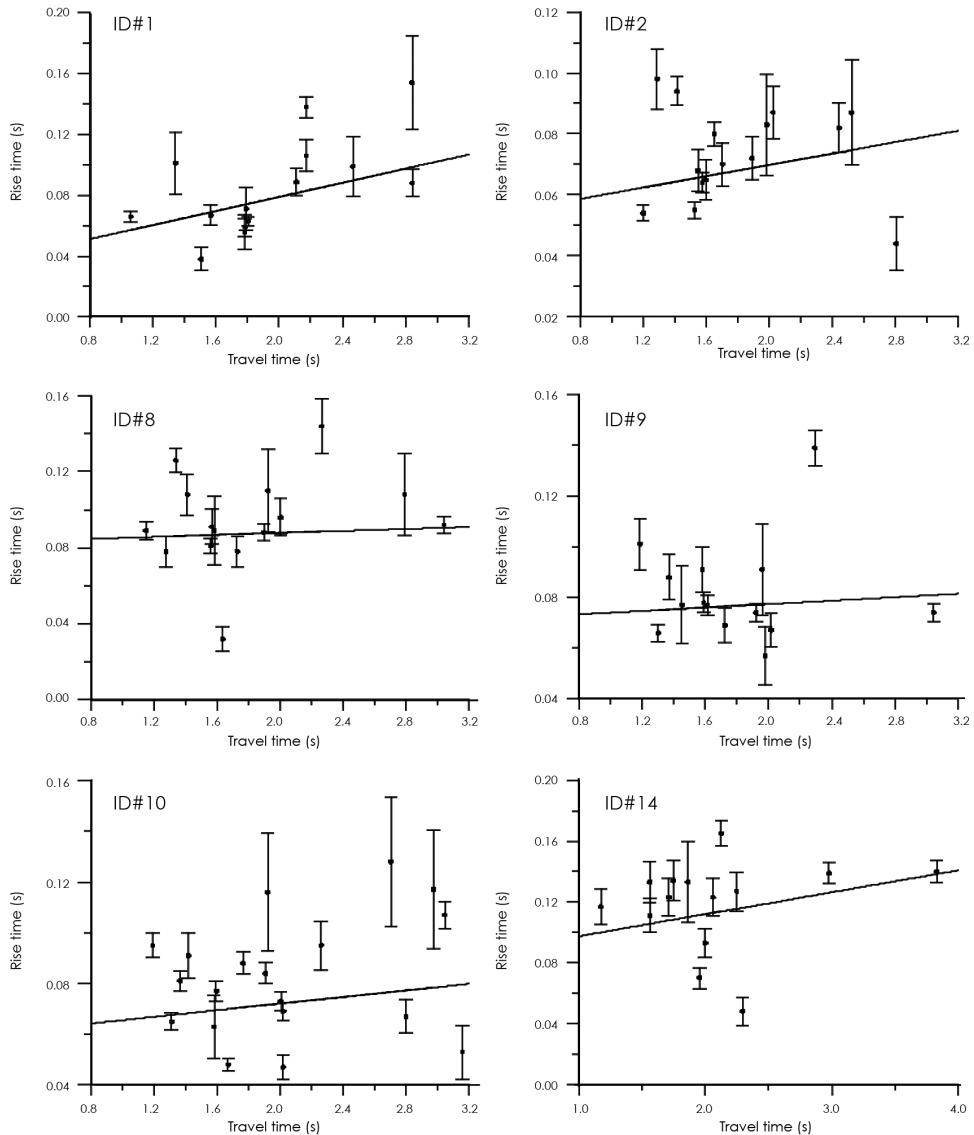
Fig. 10. Plot of rise time *versus* travel time for some studied events. On each plot the best fitting straight line, obtained from the inversion of rise times, is superimposed.

ed that a strong clustering of empirical data in a small range of values for both the considered variables induces a correlation between the regression parameters. Thus the uneven and insufficient sampling for many events could be responsible for the observed phenomenon.

Alternatively, we have to account for the limitations of the hypothesis on which the used technique is based. In fact the adopted technique uses a very simplified source model, *i.e.* an isotropic seismic source. It is known that, for a finite dimension seismic source, the directivity source effect on the rise time of first *P* waves can be described through the relationship (Zollo and de Lorenzo, 2001)

$$\tau_0 = \frac{L}{V_r}\left(1 - \frac{V_r}{V_p}\right)\sin\theta \qquad (6.1)$$

where θ is the takeoff angle (the angle formed by the tangent to the ray leaving the source and the normal to the fault plane) and V_p the *P*-wave velocity of at the source. From this equation it immediately follows that the variations of the source rise time around the non-directive source rise time given in eq. (5.4) increase with increasing the source dimension *L*. Moreover, for a directive source time function, the equation which describes the relationship between τ and Q^{-1} is non linear, as demonstrated in Zollo and de Lorenzo (2001) and de Lorenzo *et al.* (2004). In particular Zollo and de Lorenzo (2001) showed that the higher the source dimension is, the higher will be the difference between the rise times predicted by the directive source model and those predicted by eq. (3.1). In our case, all the data which are responsible for the observed correlation among τ_0 and Q_p (the data shown in the grey square of fig. 8) have been selected by AICc among the model parameters obtained from the joint inversion of τ_0 and Q_p, *i.e.* without imposing a constant stress drop for the area (fig. 9). This could imply that, above a given threshold ($\tau_0 \sim$ 30-40 ms) the directivity source effect tends to be so high to produce a non linear trend of rise times *versus* the travel time, which may result in a bad estimation of the estimated τ_0 and Q_p if one uses the linear interpolating scheme given by eq. (3.1). This result is also supported by the visual inspection of the quality of the matching of the model to data, as shown in fig. 10 for some events. It is quite evident that, even if, in some cases, an increase in rise time *versus* travel time can be observed, the dispersal of data around the best fit straight line is significantly higher than the error on data.

A possible bias in *Q* estimates could be caused by the different instrumental responses. It has to be noted that twenty-two of the available stations are equipped with Mark L4C, having an eigenfrequency of 1 Hz. The remaining two stations are equipped with Lennartz Le3D, having an eigenfrequency of 0.05 Hz. For both the two kind of stations the cutoff frequency is around 50 Hz. Since the average frequency content of the pulses ranges from 3 to 40 Hz, *i.e.* lies in the linear part of the amplitude and phase response of the instrument, we do not expect a significant distortion in amplitude of signals and phase shifting, even if the signals having the higher average frequency content (around 40 Hz) could be more sensitive to the non linear part of the instrumental response. However, only a dozen of data (fig. 3) have an average frequency higher than 30 Hz and then this problem affects only a very negligible portion of the dataset and cannot affect the obtained average *Q* estimate.

Therefore we conclude that, for the Etnean area and in the case of a limited exploration of travel times, the applicability of the classic linear rise time method has to be limited only to those earthquakes which have a source rise time less or equal to about 35 ms, at which corresponds, using a rupture velocity V_r=0.9 V_s=2.2 km/s, an average source dimension of about 80 m.

REFERENCES

AKAIKE, H. (1974): A new look at the statistical model identification, *IEEE Trans. Automatic Control*, **19**, 716-723.

AZZARO, R. and M. NERI (1992): L'attività eruttiva dell'Etna nel corso del ventennio 1971-1991. Primi passi verso la costituzione di un data-base relazionale, *CNR IIV Open File Report 3/92*.

BOURBIE, T., O. COUSSY and B. ZINSZNER (1987): *Acoustic of Porous Media* (Butterworth-Heinemann Publisher), pp. 324.

BRUNE, J.N. (1970): Tectonic stress and the spectra of seismic shear waves from earthquakes, *J. Geophys. Res.*, **75**, 4997-5009.

CAVANAUGH, J.E. (1997): Unifying the derivation for the Akaike and corrected Akaike Information Criteria, *Stat. Probabil. Lett.*, **33**, 201-208.

CAVANAUGH, J. E. and R.H. SHUMWAY (1998): An Akaike information criterion for model selection in the presence of incomplete data, *J. Stat. Plann. Infer.*, **67**, 45-65.

COCINA, O., G. BARBERI, D. PATANÈ, C. CHIARABBA and P. DE GORI (2005): Tomographic images of volatile rich magma intrusions leading to the 2001 and 2002-2003 Mt Etna eruptions, in *Proceeding of the AGU Fall Meeting*, 5-9 December 2005, San Francisco, CA, U.S.A.

DE GORI, P., C. CHIARABBA and D. PATANÈ (2005): Q_p structure of Mt. Etna: constraints for the physics of the plumbing system, *J. Geophys. Res.*, **110**, B05303, doi: 10.1029/2003JB002875.

DEICHMANN, N. (1997): Far field pulse shapes from circular sources with variable rupture velocity, *Bull. Seismol. Soc. Am.*, **87**, 1288-1296.

DE LORENZO, S. (1998): A model to study the bias on Q estimates obtained by applying the rise time method to earthquake data, in *Q of the Earth, Global, Regional and Laboratory Studies*, edited by B.J. MITCHELL and B. ROMANOWICZ, *Pure and Appl. Geophys.*, **153**, 419-438.

DE LORENZO, S. and A. ZOLLO (2003): Size and geometry of microearthquake seismic ruptures from P and S pulse width data, *Geophys. J. Int.*, **155**, 422-442.

DE LORENZO, S., A. ZOLLO and F. MONGELLI (2001): Source parameters and three-dimensional attenuation structure from the inversion of microearthquake pulse width data: Q_p imaging and inferences on the thermal state of the Campi Flegrei caldera (Southern Italy), *J. Geophys. Res.*, **106**, 16,265-16,286.

DE LORENZO, S., G. DI GRAZIA, E. GIAMPICCOLO, S. GRESTA, H. LANGER, G. TUSA and A. URSINO (2004): Source and Qp parameters from pulse width inversion of microearthquake data in southeastern Sicily, Italy, *J. Geophys. Res.*, **109**, B07308, doi: 10.1029/2003JB002577.

DEL PEZZO, E., F. BIANCO and G. SACCOROTTI (2001): Separation of intrinsic and scattering Q for volcanic tremor: an application to Etna and Masaya Volcanoes, *Geophys. Res. Lett.*, **28**, 2525-2528.

GLADWIN, M.T. and F.D. STACEY (1974): Anelastic degradation of acoustic pulses in rock, *Phys. Earth Planet. Int.*, **8**, 332-336.

GREEN, J.R. and D. MARGERISON (1978): *Statistical Treatment of Experimental Data* (Elsevier Scientific Publishing Company), pp. 392.

GRESTA, S., L. PERUZZA, D. SLEJKO and G. DI STEFANO (1998): Inferences on the main volcano-tectonic structures at Mt. Etna (Sicily) from a probabilistic seismological approach, *J. Seismology*, **2**, 105-116.

KAMPFMANN, W. and H. BERCKEMER (1985): High temperature experiments on the elastic and anelastic behaviour of magmatic rocks, *Phys. Earth Planet. Inter.*, **40**, 223-247.

KEILIS-BOROK, V.I. (1959): On estimation of the displacement in an earthquake source dimensions, *Ann. Geofis.*, **XII**, 205-214.

KJARTANSSON, E. (1979): Constant Q-wave propagation and attenuation, *J. Geophys. Res.*, **84**, 4737-4748.

LIU, H.-P., R.E. WARRICK, J.B. WESTERLUND and E. KAYEN (1994): In situ measurement of seismic shear-wave absorption in the San Francisco Holocene Bay Mud by the pulse-broadening method, *Bull. Seismol. Soc. Am.*, **84**, 62-75.

MADARIAGA, R. (1976): Dynamics of an expanding circular fault, *Bull. Seismol. Soc. Am.*, **66**, 639-666.

MARTÌNEZ-AREVALO, C., D. PATANÈ, A. RIETBROK and J.M. IBANEZ (2005): The intrusive process leading to the Mt. Etna 2001 flank eruption: constraints from 3D attenuation tomography, *Geophys. Res. Lett.*, 32, L21309, doi: 10.1029/2005GL023736.

MITCHELL, B.J. (1995): Anelastic structure and evolution of the cuntinental crust and upper mantle from seismic surface wave attenuation, *Rev. Geophys.*, **33**, 441-462.

MULARGIA, F. and R.J. GELLER (2003): Earthquake Science and Seismic Risk Reduction (Kluwer Academic Publisher), *Nato Sci. Ser. IV*, **32**, pp. 338.

PATANÈ, D. and E. GIAMPICCOLO (2004): Faulting processes and earthquake source parameters at Mt. Etna: state of the art and perspectives, in *Mt. Etna: Volcano Laboratory*, edited by A. BONACCORSO, S. CALVARI, M. COLTELLI, C. DEL NEGRO and S. FALSAPERLA, *Am. Geophys. Un., Geophys. Monogr.*, **143**, 167-189.

PATANÈ, D., F. FERRUCCI and S. GRESTA (1993): Leggi di scala e parametri di sorgente per terremoti all'Etna, in *Proceedings of the 12th GNGTS meeting*, 24-26 November 1993, Roma, Italy, 925-928.

PATANÈ, D., F. FERRUCCI and S. GRESTA (1994): Spectral features of microearthquakes in volcanic areas: attenuation in the crust and amplitude response of the site at Mt. Etna, Italy, *Bull. Seismol. Soc. Am.*, **84**, 1842-1860.

PATANÈ, D., F. FERRUCCI, E. GIAMPICCOLO and L. SCARAMUZZINO (1997): Source scaling of microearthquakes at Mt. Etna volcano and in the Calabrian Arc (Southern Italy), *Geophys. Res. Lett.*, **24**, 1879-1882.

PRESS, W.H., B.P. FLANNERY, S.A. TEUKOLSKY and W.T. VETTERLING (1989): *Numerical Recipes in Pascal: The Art of Scientific Computing* (Cambridge University Press, New York), pp. 781.

RASÀ, R., F. FERRUCCI, S. GRESTA and D. PATANÈ (1995): Etna: Sistema di alimentazione profondo, assetto, geostatica locale e bimodalità di funzionamento del vulcano, in *Progetto Etna 1993-1995*, edited by F. FERRUCCI and F. INNOCENTI (Giardini, Pisa, Italy), 145-150.

SANDERS, C.O., S.C. PONKO, L.D. NIXON and E.A. SCHWARTZ (1995): Seismological evidence for magmatic and hydrothermal structure in Long Valley caldera from local earthquake attenuation and velocity tomography, *J. Geophys. Res.*, **100**, 8311-8326.

SATO, H. and I.S. SACKS (1989): Anelasticity and thermal structure of the oceanic upper mantle: temperature calibration with heat flow data, *J. Geophys. Res.*, **94**, 5705-5715.

TONN, R. (1989): Comparison of seven methods for the

computation of Q, *Phys. Earth Planet. Inter.*, **55**, 259-268.

VASCO, D.W. and L.R. JOHNSON (1998): Whole Earth structure estimated from seismic arrival times, *J. Geophys. Res.*, **103**, 2633-2672.

WU, H. and M. LEES (1996): Attenuation structure of Coso geothermal area, California, from wave pulse widths, *Bull. Seismol. Soc. Am.*, **86**, 1574-1590.

ZOLLO, A. and S. DE LORENZO (2001): Source parameters and three-dimensional attenuation structure from the inversion of microearthquake pulse width data: method and synthetic tests, *J. Geophys. Res.*, **106**, 16,287-16,306.